# *NorSand* modelling for evaluating the triggering of flowslides in loess


Liming Zheng
*Department of Civil and Environmental Engineering – University of Alberta, Edmonton, AB, Canada*
Longde Jin
*Golder Associates (Member of WSP), Atlanta, GA, USA*
Fangzhou Liu
*Department of Civil and Environmental Engineering – University of Alberta, Edmonton, AB, Canada*

ABSTRACT
Loess contains predominately silt-sized quartz grains bonded by various cementation agents, which is of significant interest to understanding the mechanical properties of lightly cemented soils. Loess flowslides with retrogressive behaviour with liquefied slope movement and long-runout have been observed in the Heifangtai (HFT) terrace under long-term irrigation in the loess plateau of China. While the mechanism of loess flowslides has been largely ascribed to the development of flow liquefaction enhanced by the metastable structure of loess, the triggering mechanism remains unclear. This study uses finite element analysis (FEA) with PLAXIS/*NorSand* implementation to evaluate the deformation process and the triggering of flow liquefaction in the loess flowslide. The computed deformation process of the DC#2 flowslide suggests intense undrained instability initiated near the toe area of the saturated loess layer after the first failure (drained), with propagating susceptibility to flow liquefaction at the onset of the flow failure, indicating a significant strength loss due to flow liquefaction under a possible drained-to-undrained loading transition in the field.

RÉSUMÉ
Le loess contient principalement des grains de quartz de la taille d'un limon qui sont liés par divers agents de cimentation, ce qui présente un intérêt significatif pour la compréhension des propriétés mécaniques des sols légèrement cimentés. Des glissements d'écoulement de loess à comportement rétrogressif avec mouvement de pente liquéfié et long ruissellement ont été observés sur la terrasse Heifangtai (HFT) sur le plateau de loess en Chine sous irrigation à long terme. Alors que le mécanisme des glissements de flux de loess a été largement attribué au développement de la liquéfaction des flux renforcée par la structure métastable du loess, le mécanisme de déclenchement reste incertain. Cette étude utilise l'analyse par éléments finis (FEA) avec la mise en œuvre PLAXIS/*NorSand* pour évaluer le processus de déformation et le déclenchement de la liquéfaction de l'écoulement dans le glissement de loess. Les processus de déformation simulés des glissements de flux de loess DC# 2 montrent de forts effets d'instabilité non drainée initiée près de la zone d'orteil de la couche de loess saturée après la rupture initiale, avec une susceptibilité de propagation à la liquéfaction de flux au début de la rupture de flux, indiquant une force significative perte due à la liquéfaction de l'écoulement sous une éventuelle transition de chargement drainé à non drainé sur le terrain.

## 1 INTRODUCTION

Recent flow failures, such as the 2019 Brumadinho tailings dam flowslides (Robertson et al. 2019), and the 2014 Oso flowslide (Iverson and George 2015, Wartman et al. 2016), caused by natural or human activities, have shown abrupt deformation and rapid movement of flowslides with long runouts are particularly devastating to society.

Under monotonic loading, flowslides have been largely ascribed to flow instability in soils characterized by the sudden loss of strength with the development of large strains, accompanied by excess pore pressure (i.e., static or flow liquefaction). Flow liquefaction has been observed in intermediate soils, including tailings materials (Fourie et al. 2001, Carrera et al. 2011, Bedin et al. 2012) and loess (Qi et al. 2018, Xu et al. 2018, Liu et al. 2019).

As a naturally cemented silt-sized soil, loess is typically problematic upon wetting as its metastable structure can rapidly transform from a cemented soil matrix to a fluidized material. The cementation agents of loess can be salt (Fan et al. 2017), water-film (Derbyshire and Mellors 1988, Pye 1995), carbonate (Milodowski et al. 2015), or clay (Smalley et al. 2006). Researchers are not unanimous about the origins of the interparticle bonds (Barden et al. 1973, Derbyshire et al. 1995, Delage et al. 1996).

Some early reports of loess flowslide were found in Derbyshire et al. (1994); however, flow liquefaction and flow failure remain largely unexplored in the past in natural cemented soils like the Chinese loess. Qi et al. (2018) and Peng et al. (2018) documented 20 retrogressive flowslides observed in the Heifangtai (HFT) terrace, Gansu Province, China; these flowslides exhibited rapid deformation with liquefied movement, and the failures have been ascribed to flow liquefaction. Among these failures, the Dangchuan (DC) #2 loess flowslide that occurred in 2015 provides an important case history to analyze the failure mechanism of flowslides. The analyses of loess flowslides typically focus on three main aspects: 1) the mechanics of flow instability (Liu et al. 2018, 2019, 2020); 2) the triggering condition (Qi et al. 2018, Xu et al. 2018); and 3) the deformation process

based on field observation (Xu et al. 2014, Leng et al. 2018, Gu et al. 2019).

Jin et al. (Jin et al. 2022) analyzed the triggering mechanism of flow liquefaction in the DC#2 flowslide by back-calculating the shear strength considering the liquefied shear strength, $s_u$(LIQ); the results indicated that flow liquefaction was to be triggered after the initial failure, likely at the basal zone of the saturated loess layer, to propagate in the saturated base, and eventually leads to the large-scale flow failure.

The 2-D finite-element analyses using the *NorSand* model have been implemented for post-failure flow liquefaction analyses, such as the 2015 Fundão failure (Morgenstern et al. 2016, Moghaddam et al. 2020), the 2018 Cadia failure (Jefferies et al. 2019), and the 1974 Tar Island failure (Shuttle et al. 2021). Within the critical state framework, the model is effective in demonstrating the need to develop large strains with excess pore-water pressure under shearing, as they are required for maintaining equilibrium when the shear strength needed is greater than can be mobilized in the soil.

This study performs deformation analysis using finite element analysis with PLAXIS/*NorSand* implementation in the attempt to analyze the deformation process of the DC#2 flowslide. This main objective is to provide additional analyses of the failure mechanism of loess flowslides, focusing on the triggering and yielding of liquefaction.

## 2 LOESS FLOWSLIDES

### 2.1 Study Area

Heifangtai terrace is an arid loess terrace (area: ~12 km$^2$) of the Yellow River in the loess plateau of China; it consists of the Malan silty loess (thickness: 30-50 m), clay (3-20 m), and gravel (1-10 m) in sequence. The bedrock comprises sandstone with mudstone partings and the bedding plane dipping 135°∠11°. The geological setting of HFT has been detailed in several existing studies (Peng et al. 2018, Qi et al. 2018, Liu et al. 2020, Zhao et al. 2020, Xu et al. 2021). Local inhabitants were re-settled in HFT in the 1960s due to the construction of a hydropower station approx. 10 km south.

### 2.2 DC#2 Retrogressive Loess Flowslide

Xu et al. (2016) detailed the field investigation of the DC#2 loess flowslide and conducted a preliminary analysis of the failure. The work documented important field data for the deformation analysis. The field monitoring of the DC#2 flowslide indicated two failures within 4 hrs. The first failure appeared to be a localized failure, while the second was a flowslide involving a much larger mass of material. The combined failures resulted in a retreat of more than 130 m with a runout distance of 789 m (Fig. 1). The estimated total volume of the failure is 32.4×10$^4$ m$^3$.

The ground markers placed behind the scarp showed small cumulative displacements three months prior to the initial failure, which occurred around 7:50 AM on April 29, 2015, followed up by a flow failure at 10:47 AM on the same day (Qi et al. 2018). No evident deformation was found between the first failure and at least 2 hrs prior to the flow failure. The flow failure involved three individual sliding events within about 4 minutes. The first and second sliding events each resulted in about 60 m of slope retreat. The third sliding appears to be more localized and occurred on both flanks of the second sliding (Fig. 1).

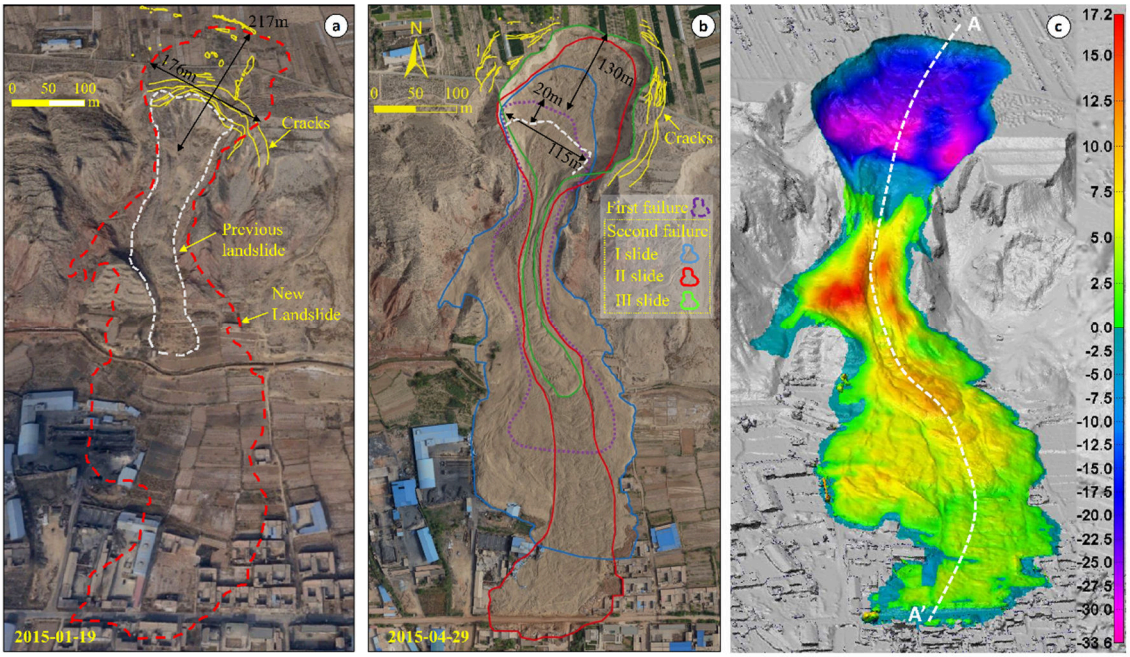


Figure 1. The DC#2 retrogressive loess flowslides occurred in HFT on April 29, 2015: a) pre-failure oblique aerial view of DC#2; b) post-failure oblique aerial view of DC#2 showing three sliding events for the retrogressive failure; and c) pre-/post-failure difference in the Digital Elevation Model with the cross-section line A-A' (after Qi et al. 2018).

## 2.3 Irrigation and Groundwater Recharge

Agricultural irrigation was started on the terrace surface by pumping water from the adjacent Yellow River in 1968, covering an area of 7.5 $km^2$ (exceeding 83% of the surface area), with annual water consumption of $6\times10^6 - 8\times10^6$ $m^3$. There is no prior knowledge of the groundwater status before irrigation.

Qi et al. (2018) reported that seepage of groundwater is commonly observed on the surface of the slope before and after failures. Liu et al. (2020) and Jin et al. (2022) also discussed the surface discharge before and after the DC#2 failure and the adjacent DC#3 flowslide. However, no information on the groundwater level was obtained before DC#2 failure or between failures. Xu et al. (2021) mapped the groundwater distribution in HFT in light of 26 electrical resistivity tomography (ERT) profiles; their results indicated that high localized GWT is associated with the crop type (i.e., irrigation cycles), affecting the failure mode. Localized high GWT with high surface discharge was found behind all reported flowslide sites in HFT.

# 3 DEFORMATION ANALYSES

The deformation analysis is conducted with finite-element analysis in PLAXIS using *NorSand*, a critical state theory-based constitutive model (Jefferies 1993).

## 3.1 Materials and Groundwater Conditions

Figure 2 presents the pre- and post-failure geometry of the DC#2 flowslide. At a depth of 20 m, the HFT loess sample has an initial void ratio range from 0.86-0.89 and a silt content (0.005-0.075 mm) of 87.9%, with a specific gravity of 2.69-2.71 and an *in situ* water content of about 8%. The average liquid and plastic limits of the samples are $w_L$ = 26.8% and $w_P$ = 17.5%, with a plastic index $PI$ = 9.3, which is slightly above the A-line and classified as CL. With a saturated water content readily over 100% and $w_C/w_L$ > 0.85, the HFT loess is susceptible to liquefaction based on the criteria proposed by Bray and Sancio (2006).

Liu et al. (2019) showed a state-dependent effect of structure on the flow behaviours of the HFT loess using the conventional undrained triaxial tests, i.e., the metastable structure can either facilitate or impede the onset of flow liquefaction. Such a state-dependency can be attributed to the offset of critical state lines (CSL) between the intact and reconstituted loess samples in the $e$:ln$p'$ plane. Similar CSL offsets were reported for other Chinese loess samples (Xu and Coop 2016, 2017, Xu et al. 2018).

Additional isotropically consolidated undrained tests (CIU) data confirms the intense strain-softening behaviour of the HFT loess with positive state parameters (Qi et al. 2018). The critical state friction angle of intact HFT loess samples is tested as 33.7° for samples collected at a depth of 20 m (Liu et al. 2019) and 34.1° for 30 m (Xu et al. 2018). The strength parameters of soils are set to be the same as in the previous study (Jin et al. 2022), as listed in Table 1.

Table 1. Summary of the Mohr-Coulomb parameters

| Material | $\gamma$ (kN/m$^3$) | $c$ (kPa) | $\phi$ (°) | $E$ (MPa) |
|---|---|---|---|---|
| Loess (dry) | 15 | 20 | 33 | 11 |
| Loess (saturated) | 19.5 | 0 | 33 | 11 |
| Silty clay | 20 | 10 | 30 | 12 |
| Sandy gravel | 20 | 0 | 40 | 35 |
| Bedrock | 20 | - | - | - |

While the information on the groundwater condition and the distribution of void ratio and state parameter is extremely limited prior to the failure, the relatively uniform property of loess has provided some confidence in assessing the field conditions from laboratory tests.

## 3.2 *NorSand* Parameters and Calibration

Liu et al. (2020) calibrated the *NorSand* model for the intact and reconstituted silty HFT loess under low-stress levels. The *NorSand* parameters are listed in Table 2. Several approximations are needed; for example, a curved CSL is idealized to fit the samples, and the effect of the structure is replicated by introducing an overconsolidation ratio (OCR) of 1.5. The output data from the Visual Basic (VB)-based *NorSand* simulation is similar to the results from the PLAXIS-based *NorSand* simulation using the same parameters, as illustrated in Figure 3.

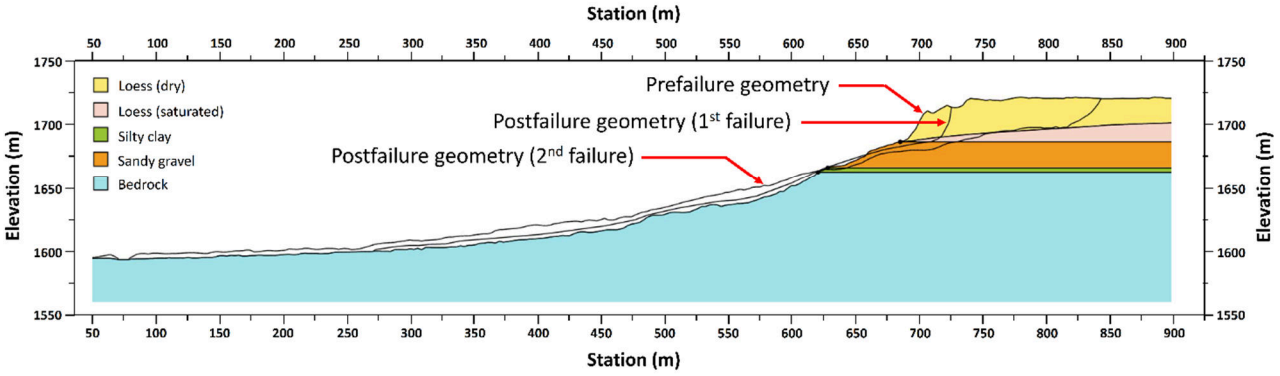


Figure 2. Simplified pre-failure geometry overlaying the approximate post-failure geometries of the first and second (flow) failures of the DC#2 loess flowslide for deformation analysis (location of the cross-section profile A-A' shown in Fig. 1).

Table 2. Summary of *NorSand* model parameters

| Parameter | Definition | Loess (saturated) |
|---|---|---|
| $G_{\mathrm{ref}}$ | Shear modulus at the reference pressure | 7 MPa |
| $p_{\mathrm{ref}}$ | Reference mean pressure | 101 kPa |
| $n_G$ | Exponent of the power-law elasticity | 1 |
| $\nu$ | Poisson's ratio | 0.2 |
| $C_a$ | Void ratio corresponding to a mean pressure equal to 0 kPa | 0.965 |
| $C_b$ | Parameter of the power-law expression | 0.29 |
| $C_c$ | Exponent of the power-law | 0.27 |
| $M_{tc}$ | Critical state stress ratio | 1.36 |
| $N$ | Numerical coupling coefficient | 0.3 |
| $\chi_{tc}$ | State-dilatancy coefficient | 3.5 |
| $H_0$ | Hardening parameter | 100 |
| $H_\psi$ | Hardening parameter | 0 |
| $S$ | Softening parameter | 1 |
| $\psi_0$ | Initial value of the state parameter | 0.078 |

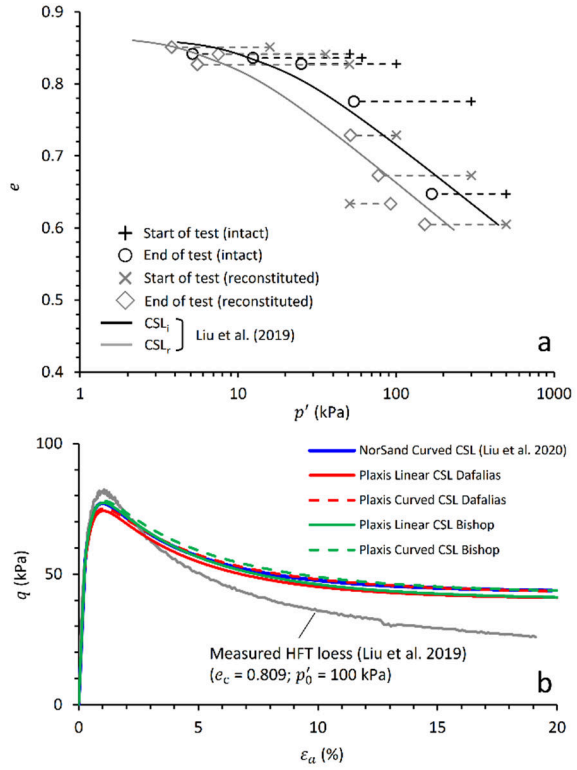


Figure 3. a) The CSLs used for modelling the undrained behaviours of the HFT loess (both intact and reconstituted specimens are included) (after Liu et al. 2019) and b) Calibration of undrained behaviours of intact HFT loess at $p'_0$ = 100 kPa with the difference between VB-based and PLAXIS-based *NorSand* simulation.

## 4 RESULTS AND INTERPRETATION

The deformation analysis focuses on the state of the slope immediately after the first failure under drained conditions. As discussed in Jin et al. (Jin et al. 2022), the first failure is the result of the gradual deformation with increasing GWT due to long-term irrigation with a Factor of Safety (FoS) reduced from 1.17 (without a perched GWT) to 1.02 (with GWT at 1690 m-MSL, i.e., 5 m of saturated loess layer).

Similar to the observation by Jin et al. (Jin et al. 2022), the loess slope was in an unstable state immediately after the first failure, with an evident critical slip surface as illustrated by the incremental deviatoric strain (Fig. 4).

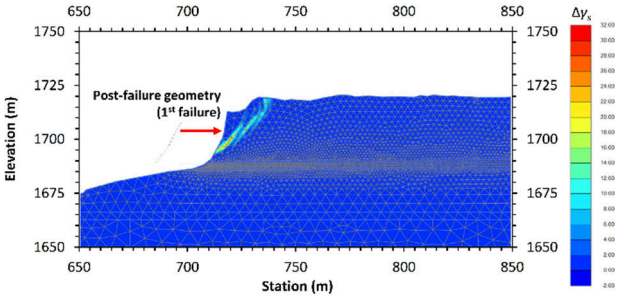


Figure 4. The incremental deviatoric strain $\Delta\gamma_s$ immediately after the first failure.

It is postulated that the loess slope must respond to the 'debuttressing' due to the first failure near the toe area. This provides a possibility for lateral movement at this location, which leads to strain-weakening propagating upwards into the saturated loess layer. In addition to this possible lateral movement, the first failure will introduce a new hydraulic gradient and result in the convergence of groundwater behind the scarp of the first failure.

Qi et al. (2018) proposed that the displaced materials of the first failure may deposit near the toe area with such a localized failure, and thus the displaced material may impede the existing seepage points, introducing a 'drained-to-undrained' loading transition; while this hypothesis can provide a sound explanation on the undrained triggering condition, the deformation analyses results showed that such a deposit is not necessarily a triggering mechanism.

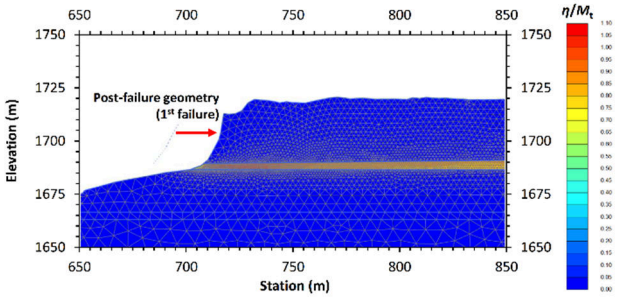


Figure 5. Distribution of controlling stress ratio in the DC#2 flowslide after the first failure.

The normalized stress ratio, $\eta/M_t$, reflects the degree of mobilization of the strength of the soil (Fig. 5). A value of

unity for this ratio indicates that the soil has reached the critical state with continuous deformation at constant load. The red zone indicates that the failure initiates at the toe area and propagates throughout the saturated loess layer. The plastic points in PLAXIS confirm the likely locations of liquefaction near the toe area, as shown in Fig. 6.

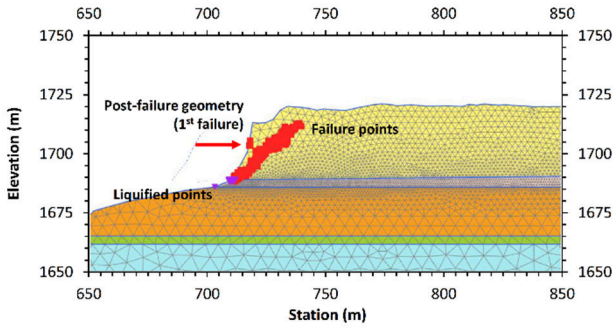


Figure 6. Plastic points of the DC#2 flowslide after the first failure.

These findings are consistent with the observations based on the back-calculation using the limit equilibrium method (Jin et al. 2022) with a liquified shear strength, $s_u$(LIQ) = 0.073-0.09 $\sigma'_{v0}$ (Fig. 7).

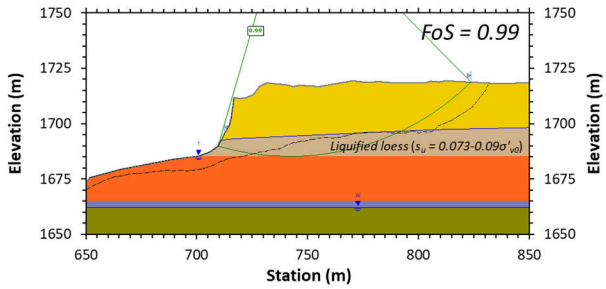


Figure 7. The critical slip surface of the fully-softened loess under an undrained condition with a retreat of the scarp of approx. 120 m behind the first failure (after Jin et al. 2022).

## 5 DISCUSSION AND CONCLUSIONS

The failure process and mechanism of the loess flowslides in HFT are revisited using a finite-element analysis approach with the PLAXIS/*NorSand* implementation. In addition to the comparison with the back-analysis using the limit equilibrium method in our previous study (Jin et al. 2022), a preliminary understanding of the deformation analysis is gained on the triggering mechanism of flow liquefaction for the DC#2 loess flowslide.

The results have indicated that liquefaction initiated near the toe after the first failure; the first failure provided the triggering condition for the onset of liquefaction by permitting the lateral movement of the toe due to the 'de-buttressing' effect. This possible lateral movement reflects the need to develop large strains with excess pore-water pressure under shearing, as they are required for maintaining equilibrium when the shear strength needed is greater than can be mobilized in the soil. The results match the observation of flowslide initiation by Eckersley (1990), highlighting the need for an initial failure, followed by the subsequent development of excess pore-water pressure and flow liquefaction.

Current failure analysis heavily relies on assumptions based on field observation and surface-based geological surveys without the aid of accurate subsurface information. Geotechnical exploration is highly recommended to justify the subsurface conditions, including groundwater level changes and the *in situ* tests of soil strength are needed to prevent further landslides in HFT.

## ACKNOWLEDGEMENT

The authors acknowledge the financial support of the NSERC Discovery Grant and the start-up fund from the Faculty of Engineering at the University of Alberta. The authors express gratitude for the invaluable input and discussion with Dr. Qiang Xu at the Chengdu University of Technology and with Dr. Kuanyao Zhao at the Huanghuai University. The assistance for the field investigation from the students at the Chengdu University of Technology is greatly appreciated.

## REFERENCES

Barden, L., McGown, A., and Collins, K. 1973. The collapse mechanism in partly saturated soil. Engineering Geology, **7**(1): 49–60.

Bedin, J., Schnaid, F., Da Fonseca, A.V., and Costa Filho, L.D.M. 2012. Gold tailings liquefaction under critical state soil mechanics. Géotechnique, **62**(3): 263–267. doi:10.1680/geot.10.P.037.

Bray, J.D., and Sancio, R.B. 2006. Assessment of the liquefaction susceptibility of fine-grained soils. Journal of geotechnical and geoenvironmental engineering, **132**(9): 1165–1177. American Society of Civil Engineers.

Carrera, A., Coop, M., and Lancellotta, R. 2011. Influence of grading on the mechanical behaviour of Stava tailings. Géotechnique, **61**(11): 935–946. doi:10.1680/geot.9.P.009.

Delage, P., Audiguier, M., Cui, Y.-J., and Howat, M.D. 1996. Microstructure of a compacted silt. Canadian Geotechnical Journal, **33**(1): 150–158. NRC Research Press.

Derbyshire, E., Dijkstra, T.A., Smalley, I.J., and Li, Y. 1994. Failure mechanisms in loess and the effects of moisture content changes on remoulded strength. Quaternary International, **24**(C): 5–15. doi:10.1016/1040-6182(94)90032-9.

Derbyshire, E., and Mellors, T.W. 1988. Geological and geotechnical characteristics of some loess and loessic soils from China and Britain: A comparison. Engineering Geology, **25**(2–4): 135–175. doi:10.1016/0013-7952(88)90024-5.

Derbyshire, E., Meng, X., Wang, J., Zhou, Z., and Li., B. 1995. Collapsible loess on the loess plateau of China. *In* Genesis and Properties of Collapsible Soils. Springer Netherlands. pp. 267–293.

Eckersley, D. 1990. Instrumented laboratory flowslides. Géotechnique, **40**(3): 489–502. Thomas Telford Ltd.

Fan, X., Xu, Q., Scaringi, G., Li, S., and Peng, D. 2017. A chemo-mechanical insight into the failure mechanism of frequently occurred landslides in the Loess Plateau, Gansu Province, China. Engineering Geology, **228**(June): 337–345. doi:10.1016/j.enggeo.2017.09.003.

Fourie, A.B., Blight, G.E., and Papageorgiou, G. 2001. Static liquefaction as a possible explanation for the Merriespruit tailings dam failure. Canadian Geotechnical Journal, **38**(4): 707–719. doi:10.1016/j.soildyn.2005.02.011.

Gu, T., Zhang, M., Wang, J., Wang, C., Xu, Y., and Wang, X. 2019. The effect of irrigation on slope stability in the Heifangtai Platform, Gansu Province, China. Engineering Geology, **248**: 346–356. Elsevier.

Iverson, R.M., and George, D.L. 2015. Modelling landslide liquefaction, mobility bifurcation and the dynamics of the 2014 Oso disaster. Géotechnique, **66**(3): 175–187. Thomas Telford Ltd.

Jefferies, M. 1993. Nor-Sand: a simle critical state model for sand. Géotechnique, **43**(1): 91–103. Thomas Telford Ltd.

Jefferies, M., Morgenstern, N.R., Van Zyl, D., and Wates, J. 2019. Report on NTSF Embankment Failure.

Jin, L., Zheng, L., Fuggle, A., and Liu, F. 2022. Back-analzying the triggering of a retrogressive loess flowslide. *In* Geohazards 8. p. (in press).

Leng, Y., Peng, J., Wang, Q., Meng, Z., and Huang, W. 2018. A fluidized landslide occurred in the Loess Plateau: A study on loess landslide in South Jingyang tableland. Engineering Geology, **236**(4): 129–136. doi:10.1016/j.enggeo.2017.05.006.

Liu, F., Frost, J., Macedo, J., and Xu, Q. 2020. Effects of structure on the mechanical behavior of loess: implications for flowslides in cemented soils. *In* Proceedings of the 73rd Canadian Geotechnical Conference (GeoVirtual 2020).

Liu, F., Xu, Q., Zhang, Y., Frost, J.D., and Zhang, X. 2019. State-dependent flow instability of a silty loess. Géotechnique Letters, **9**(1): 22–27.

Liu, F., Xu, Q., Zhang, Y., Xiu, D., Zhao, K., and Frost, J.D. 2018. Effects of grading on the flow behaviors of saturated loess. *In* Proceedings of International Symposium on “Geomechanics from Micro to Macro in Research and Practices (IS Atlanta)". p. (in press).

Milodowski, A.E., Northmore, K.J., Kemp, S.J., Entwisle, D.C., Gunn, D.A., Jackson, P.D., Boardman, D.I., Zoumpakis, A., Rogers, C.D.F., Dixon, N., Jefferson, I., Smalley, I.J., and Clarke, M. 2015. The mineralogy and fabric of ‘Brickearths’ in Kent, UK and their relationship to engineering behaviour. Bulletin of Engineering Geology and the Environment, **74**(4): 1187–1211. doi:10.1007/s10064-014-0694-5.

Moghaddam, R., Riveros, G., and Farhangi, S. 2020. A Finite Element Analysis of the Fundão Dam Failure. *In* GeoVirtual 2020.

Morgenstern, N.R., Vick, S.G., Viotti, C.B., and Watts, B.D. 2016. Report on the Immediate Causes of the Failure of the Fundão Dam. *In* Fundão Tailings Dam Review Panel.

Peng, D., Xu, Q., Liu, F., He, Y., Zhang, S., Qi, X., Zhao, K., and Zhang, X. 2018. Distribution and failure modes of the landslides in Heitai terrace, China. Engineering Geology, **236**(June 2016): 97–110. Elsevier. doi:10.1016/j.enggeo.2017.09.016.

Pye, K. 1995. The nature, origin and accumulation of loess. Quaternary Science Reviews, **14**(7–8): 653–667. doi:10.1016/0277-3791(95)00047-X.

Qi, X., Xu, Q., and Liu, F. 2018. Analysis of retrogressive loess flowslides in Heifangtai, China. Engineering Geology, **236**: 119–128. doi:10.1016/j.enggeo.2017.08.028.

Robertson, P.K., de Melo, L., Williams, D.J., and Wilson, G.W. 2019. Report of the expert panel on the technical causes of the failure of Feijão dam I. Commissioned by Vale,: 81.

Shuttle, D., Marinelli, F., Brasile, S., and Jefferies, M. 2021. Validation of computational liquefaction for tailings: Tar Island slump. Geotechnical Research, **40**(XXXX): 1–24. Thomas Telford Ltd.

Smalley, I.J., Mavlyanova, N.G., Rakhmatullaev, K.L., Shermatov, M.S., Machalett, B., O’Hara Dhand, K., and Jefferson, I.F. 2006. The formation of loess deposits in the Tashkent region and parts of Central Asia; and problems with irrigation, hydrocollapse and soil erosion. Quaternary International, **152**: 59–69. doi:10.1016/j.quaint.2006.02.018.

Wartman, J., Montgomery, D.R., Anderson, S.A., Keaton, J.R., Benoît, J., dela Chapelle, J., and Gilbert, R. 2016. The 22 March 2014 Oso landslide, Washington, USA. Geomorphology, **253**: 275–288. Elsevier.

Xu, L., and Coop, M.R. 2016. Influence of structure on the behavior of a saturated clayey loess. Canadian Geotechnical Journal, **53**(6): 1026–1037. NRC Research Press.

Xu, L., and Coop, M.R. 2017. The mechanics of a saturated silty loess with a transitional mode. Géotechnique, **67**(7): 581–596. doi:10.1680/jgeot.16.P.128.

Xu, L., Coop, M.R., Zhang, M.S., and Wang, G. 2018. The mechanics of a saturated silty loess and implications for landslides. Engineering Geology, **236**(5): 29–42. Elsevier.

Xu, L., Dai, F.C., Tu, X.B., Tham, L.G., Zhou, Y., and Iqbal, J. 2014. Landslides in a loess platform, North-West China. Landslides, **11**(6): 993–1005. doi:10.1007/s10346-013-0445-x.

Xu, Q., Peng, D., Qi, X., Dong, X., Li, H., and Ju, Y. 2016. Dangchuan *2#* Landslide of April 29, 2015 in Heifangtai Area of Gansu Province: Characteristics and Failure Mechanism. Journal of Engineering Geology, **24**(2): 167-180 (in Chinese).

Xu, Q., Zhao, K., Liu, F., Peng, D., and Chen, W. 2021. Effects of land use on groundwater recharge of a loess terrace under long-term irrigation. Science of The Total Environment, **751**: 142340. Elsevier.

Zhao, K., Xu, Q., Liu, F., Xiu, D., and Ren, X. 2020. Field monitoring of preferential infiltration in loess using time-lapse electrical resistivity tomography. Journal of Hydrology, **591**: 125278. Elsevier.